Selection of temperature and power parameters for multi-modular lunar jet penetrator

Vladimir A. ZAGOVORCHEV*,[1], Olga V. TUSHAVINA[2]

*Corresponding author
*,[1]Department of Managing Exploitation of Space-Rocket Systems,
Aerospace Institute, Moscow Aviation Institute (National Research University),
4 Volokolamskoe Highway, Moscow 125993, Russian Federation,
zagovorchev@mai.ru
[2]Aerospace Institute, Moscow Aviation Institute (National Research University),
4 Volokolamskoe Highway, 125993, Moscow, Russian Federation,
solgtu@gmail.com

DOI: 10.13111/2066-8201.2019.11.S.23

Received: 13 April 2019/ Accepted: 05 June 2019/ Published: August 2019

Abstract: *The questions and the particularity of the choice of design parameters of multi-module lunar jet penetrators are considered. A constructive layout of the penetrator is proposed and the advantages of a multi-modular design are presented. In particular, the limitation on the depth of penetration of the reactive penetrator of the standard scheme, associated with the characteristics of the flow of combustion products from the nozzle into a variable length channel left after the passage of the apparatus, is described. An algorithm is suggested for solving the problem of design parameters of multi-module lunar jet penetrators, which is based on the same methods for finding design parameters of single-module penetrators. Nonetheless, in this case, among the main design parameters that uniquely determine the appearance of both individual modules and the apparatus as a whole, in addition to pressure in the combustion chamber, elongation, pressure relationships at the nozzle and in the chamber, engine running time in air, structural mass and angle, contents of the head including, multiple modules (or sections of the remote control) of the device. By the above method, the calculation of the gas-dynamic parameters for the operation process in solid propellant rocket engines was carried out. Critical temperatures of solid fuel and pressure in the combustion chamber are limited by the ones leading to destruction of the engine and the penetrator.*

Key Words: *penetrator, moon, regolith, solid propellant rocket engine, gas dynamics*

1. INTRODUCTION

Theoretical and experimental studies on the creation of single-module ground reactive penetrators showed [1], [2], [3], [4], [5], [6], [7], [8], [9], [10], [11], [12], [13], [14], [15], [16], [17], [18], [19], [20], [21], [22] that such penetrators, by their design features, as well as intra-chamber processes, occurring during the period of work of the propulsion system, have a number of disadvantages that can significantly affect their application.

Firstly, to create high values in frontal thrust, single-module lunar (LRP) penetrators should use rocket engines with solid fuel of high elongation and high loading density, and this leads to an increase in pressure in the combustion chamber, the appearance of erosive combustion of fuel and, consequently to reduction of reliability of solid propellant rocket

engines [23]. Secondly, single-module LRPs have a limited penetration depth, since, with a length of movement in the ground more than 230 ... 260 calibers (with a constant mass flow rate of combustion products), the compression shock will "rest" at the nozzle edge. Meaning that a subsonic gas flow will be concentrated in the well, and a further increase in the penetration depth will lead to a jump in the critical section of the nozzle into the combustion chamber, which will destroy the engine.

The mentioned disadvantages of single-module LRP can be eliminated by using multi-modular ground-effect reactive penetrators, including a combination of several solid fuel sections arranged in series along the axis, and a body that surrounds the sections, having a head at one end, and a nozzle at the other end. One of the options of the structural layout of the multi-module lunar jet penetrator is presented in Fig. 1.

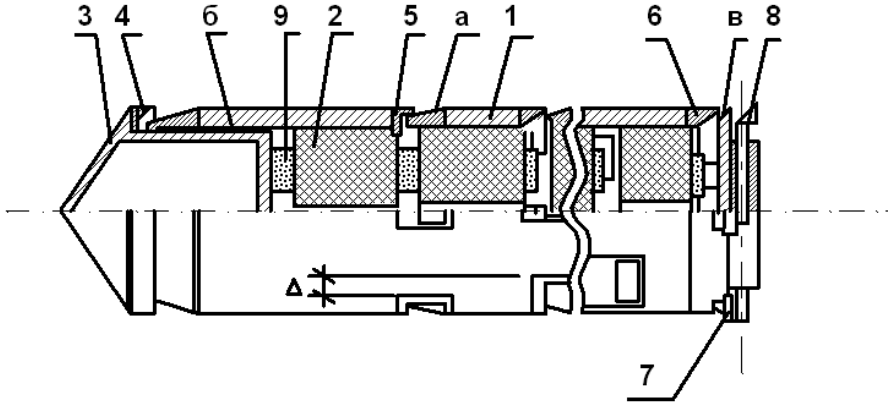

Fig. 1 – Structural scheme of a multi-modular LRP with a payload located in the head
1– body; 2 – section TT; 3 – the head; 4 – annular nozzle; 5 – insertion; 6 – multi-node unit; 7 – device closing nozzle openings; 8 – stop; 9 – igniter; "A" – nozzle groove; "B" – the gap; "In" – nozzle hole

It should be noted that the individual elements of a multi-modular lunar jet penetrator can be equipped with solid fuel sections, differing both in size, configuration, and physic-chemical characteristics. In this case, each LRP module has a specific total impulse value, which is determined by variation of engine thrust of a separate section in terms of time and duration of its operation. By controlling the order of operation of solid-propellant rocket engines of individual modules, it is possible to provide the required traction and dynamic characteristics in different parts of the trajectory of the lunar jet penetrator.

2. METHODOLOGY

To find solution for the problem of choosing the design parameters of multi-module lunar jet penetrators, the same methods are used as for finding the design parameters of single-module LRP [24], [25], [26]. Nonetheless, in this case, among the main design parameters that uniquely determine the appearance of both individual modules and LRP as a whole, in addition to pressure in the combustion chamber, elongation, pressure ratio at the nozzle section and in the chamber, engine running time, mass of the structure and angle of head part, additionally incudes the number of modules (or control sections) of lunar jet penetrator.

The design parameters are found separately for each module, and the general scheme for selecting the optimal design parameters of multi-modular soil reactive penetrators is shown in Fig. 2.

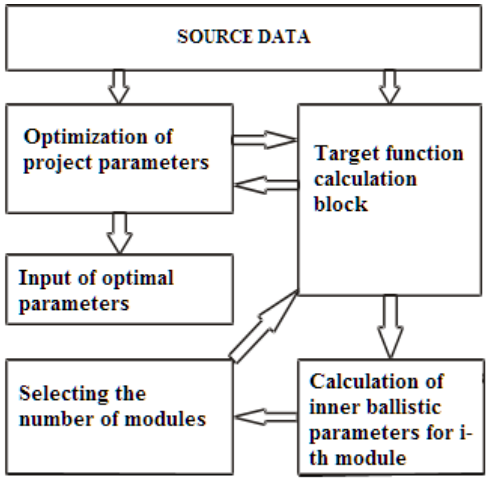

Fig. 2 – General diagram for choosing the optimal parameters of a multi-modular LRP

From the set of design parameters of the lunar reactive penetrator, it is necessary to choose the main design parameters that uniquely determine an alternative construction-design solution. Definitely, for each set of design parameters there will be some optimal (in terms of reaching the maximum penetration depth) condition determined by the speed and angle of the penetrator entering the ground, procession angles, nutation and proper rotation, the angle between the penetrator velocity vector and its longitudinal axis etc.

At the same time, the choice of the optimal launch option is significantly influenced by the restrictions imposed on the parameters of the penetrator and its trajectories. So, it is necessary to make a simultaneous selection of the design parameters of a multi-module lunar jet penetrator and parameters characterizing the conditions for its launch. Therefore, for each considered construction arrangement of the module, the system of basic design and initial parameters consists of three groups of quantities: a) parameters that describe the physical and mechanical properties of soils; b) parameters of the launch conditions; c) parameters that fully determine the construction of the penetrator.

If other things are equal, the totality of these quantities makes it possible to construct a mathematical model of the process of launching a multi-module lunar jet penetrator into the lunar soil with various methods for its launch.

3. RESULTS AND DISCUSSIONS

3.1 Model for calculation of the gas-dynamic parameters of the i-th module of the lunar jet penetrator

In the case [27], when an engine of a specific design scheme is defined, structural materials with given mass and strength characteristics are selected, fuel is selected and all its physical and chemical characteristics are indicated, in the first approximation the parameters of a single solid propellant rocket engine can be determined through the nominal pressure in the combustion chamber P_K^H the outer diameter of the combustion chamber D_H body extension λ_δ and the pressure ratio at the nozzle exit p_a to the pressure in the chamber $\xi = \frac{P_a}{P_K}$ in the following functional sequence. For a given nominal pressure in the combustion chamber, the pressure at each moment of time will be:

$$P_K = \frac{K_P P_K^H}{t} t \quad at \quad 0 \le t \le t_1, \quad P_K = P_K^H \quad at \quad t_2 \le t \le t_2$$

$$P_K = K_P P_K^H - \left[\frac{K_P P_K^H - P_H}{t_2 - t_1}(t - t_1)\right] \quad at \quad t_1 \le t \le t_2 \tag{1}$$

$$P_K = P_K^H - \frac{P_K^H}{t_4} t \quad at \quad t_3 \le t \le t_4,$$

where $t_1 + t_2 + t_3 + t_4 = T$ – is total time of work of solid propellant solid fuel rocket engine t_1 – is time of pressure rise from zero to maximum, t_2 – is time of pressure drop from peak to nominal; t_3 – is engine running time with constant pressure; t_4 – is burnout time; K_p – is pressure decrease ratio.

Solid propellant charge fills not only the cylindrical volume of the body, but also can partially enter into the space formed by the bottom of the combustion chamber, therefore the length of the fuel block can be l_1 determined by dependency

$$l_1 = D_H(\lambda_\delta + C_1) \tag{2}$$

where C_1 – is dimensionless ratio taking into account the partial filling of the bottom volume with fuel.

To find the traction and flow characteristics of the engine, we need to find the average surface of burning S_Γ

$$S_\Gamma = \pi C_2 l_1 D_H \tag{3}$$

where C_2 – ratio determined by the form of charge.

The burning speed at a given pressure in the combustion chamber, depending on the type of fuel, is found [28] by either a linear law of combustion or a power law of combustion. In general, these dependencies can be represented as

$$u = a + \text{ℬ} P_K \tag{4}$$

or

$$u = u_1 + P_K^\nu \tag{5}$$

where a, ℬ, u_1, ν – are empirical coefficients that depend on the type of fuel.

Once we know the burning surface and the burning speed of the fuel, it is possible to calculate in a first approximation arrival of gases into the combustion chamber per second

$$\dot{M} = \rho_T u S_\Gamma \tag{6}$$

where ρ_T – is fuel density.

To put the penetrator into the ground at a certain depth, the LRP needs some total thrust impulse

$$I_\Sigma = \int_0^T R(t)dt \tag{7}$$

where $R(t)$ and t are thrust and engine running time.

This useful total impulse must be provided by the engine impulse.

$$I_{\Sigma} = \int_{0}^{M_T} I_{ed} dM \tag{8}$$

where M_T – is the initial mass of the fuel.

If the average value of a single impulse I_{ed} we know the required mass of fuel, which will ensure the creation of a given total impulse, which will be

$$M_T = \frac{I_{\Sigma}}{I_{ed}} \tag{9}$$

Value I_{ed} depends on the selected fuel and engine performance

$$I_{ed} = I_1 + I_2\left(1 - \frac{P_H}{\xi P_K^H}\right), \tag{10}$$

where I_1, I_2 – are components of a single impulse; ξ – is the ratio of pressure at the nozzle exit to pressure in the chamber, which are independent of pressure; P^H – is external pressure.

Thrust of i -th engine module in the first approximation can be expressed in terms of the charge combustion parameters [29] provided that the mass coming from fuel combustion equals the flow through the nozzle.

$$R=I_{ed}\, P_t\, uS_t \tag{11}$$

To create the required pressure in the combustion chamber for a given burning surface, it is necessary to establish the area of nozzle section

$$S_{KP} = \left(\frac{a}{P_K} + \text{б}\right)\rho_T \beta_\Gamma S_\Gamma \text{ – for the linear law of burning;} \tag{12}$$

$$S_{KP} = u_1 P_K^{\nu-1}\rho_T \beta_\Gamma S_\Gamma \text{ – for the power law of burning.} \tag{13}$$

where β_Γ – is specific pressure impulse characterizing the thermodynamic properties of the fuel. The broadening of the nozzle is determined by the coefficient of the pressure at the nozzle exit to the pressure in the combustion chamber.

$$x = \frac{d_a}{d_{KP}} = \sqrt{\frac{\left(\frac{2}{K+1}\right)^{\frac{1}{K-1}}\sqrt{\frac{K-1}{K+1}}}{\xi^{\frac{2}{K}} - \xi^{\frac{K+1}{K}}}} \tag{14}$$

where K is the adiabatic index; d_a – the diameter of nozzle; d_{KP} – diameter of critical area of the nozzle. Knowing the diameter of the critical area, we can determine the diameter of the fuel channel

$$d_{\text{б}} = K_d d_{KP}, \tag{15}$$

where K_d - is dimensionless coefficient that determines the ratio of the diameter of the channel at the beginning of the engine to the diameter of the nozzle.

For the charge of the regular form, the magnitude of the set of fuel is equal to

$$e = \frac{D_0 - d_{\text{б}}}{4} \tag{16}$$

where D_0 – is outer diameter of the fuel charge, determined by the expression

$$æ = \frac{4eD_0}{D_б^2 - D_0^2} \tag{17}$$

where æ is Pobedonostsev's criterion, indicating the velocity of gases along the charge (it depends on the pressure in the combustion chamber and the higher it is allowed, the higher is the pressure in chamber); $D_б$ – is internal diameter of the combustion chamber.

When we know the rate of burning of fuel at a given average pressure in the combustion chamber and the size of the surface, it is possible to estimate in a first approximation the time of engine operation

$$T = \frac{e}{u} \tag{18}$$

From the theory of solid propellant rocket engines, it is known [30] that the charge mass can be calculated by the formula

$$M_K = \sum_{i=1}^{n} M_{K_i}, \tag{19}$$

where M_{K_i} is the mass of the i – th engine module:

$$M_K = M_T \left[2K_b \frac{P_K}{\Delta\sigma_б} \frac{P_K}{\rho_T}\left(1 + \frac{0{,}6}{\lambda_K}\right)\left(1 + \frac{12}{M_T}\right) + \frac{200}{\Delta\rho_T\lambda_b} + \frac{0.002I_{ed}}{T}\right] \tag{20}$$

where K_b – is reduced safety factor; Δ – is the fill factor of the cross section of combustion chamber; $\sigma_б$, ρ_K – is strength and density of the material of the body.

The total mass of the penetrator for movement in the ground consists of the mass of the payload, the mass of the structure and the mass of fuel

$$M_0 = M_{pn} + \alpha M_K + \sum_{i=1}^{n} M_{T_i}, \tag{21}$$

where α – is coefficient taking into account the mass of the head part of the LRP; M_{T_i} is the mass of fuel of the i -th module.

Head extension may be defined as a cone.

$$\lambda_K = \frac{1}{2tg\beta}, \tag{22}$$

where β – the angle of the semi-cone.

Nozzle extension for the engine

$$\lambda_c = \frac{I_c}{D_H}, \tag{23}$$

where l_c=C_3[C_4+(ξ-1)C_5]/2$tg\beta_{ex}$×D_{kp} – is nozzle length; C_3, C_4, C_5 – are dimensionless coefficients taking into account the configuration of the nozzle; β_{ex} – half the angle of the opening of the nozzle outlet.

The full extension of the LRP consists of an elongated head, a body and a nozzle.

$$\lambda = \lambda_K + \lambda_b + \lambda_C \tag{23}$$

The results of calculation of the parameters of the internal ballistics for the lunar penetrator.

As an example for the abovementioned method, the gas dynamic parameters of the working process in solid propellant rocket engines using the initial data presented in Table 1

were calculated, and the calculation results are presented in the form of graphs in Fig. 3 – 6. Calculations were performed for different values:

– charge temperatures T_3 = -20^{0}C… + 20^{0}C;

– fuel charge lengths l_3 = 0.5 ... 1.25 m;

– nozzle diameters d_{KP} = 0.017 ... 0.018 m;

– Poisson's ratio for fuel material μ = 0.35 ... 0.05.

Table 1. – The source data for the numerical example

Symbol	R	f_p	λ_P	K_L	ρ_T	Δ	D_{KC}	a	D_0
Dimension	kcal/mol*kg*deg	kg*m/kg	-	-	Kg*m^3	-	m	m^3/kg	M
Value	36	95,000	0.15	2	1700	0.98	0.044	0,003	0.04
Symbol	K	n_z	μ_u	B_t	E	a	d	$\mathscr{b}$	χ
Dimension	-	-	-	-	kg/m^2	cm/s	cm^3/s*kg	m	-
Value	1.25	1	0.98	320	2.5×10^7	0.3	0,0063	0,008	0.94

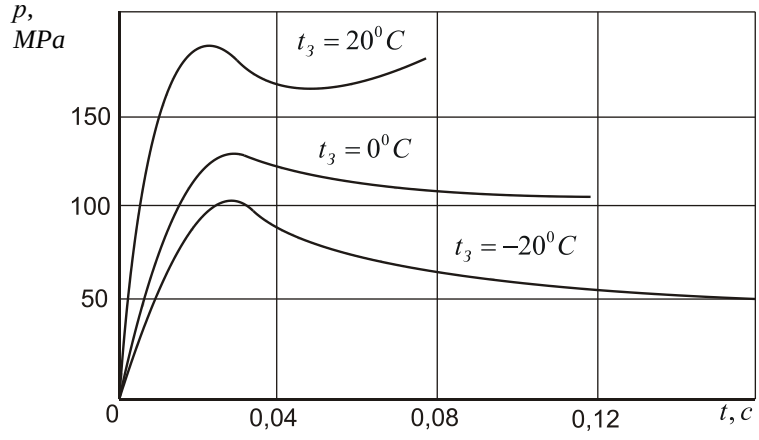

Fig. 3 – The change in pressure in the CC in time for different values of initial temperatures

Analysis of the results indicates a strong influence of the temperature charge on the nature and magnitude of the working pressure in the combustion chamber and the pressure drop near the bottom and nozzle.

At charge temperature T_3 = -20^{0}C maximum pressure in the combustion chamber is P_{MAX} = 105 MPa, and the maximum drop at the bottom and the nozzle ΔP_{MAX} = 15 MPa, which much different from the values of these quantities at T_3 = +20^{0}C, respectively, P_{MAX} = 180 MPa and ΔP_{MAX}= 18 MPa.

An experimental test showed that launching of the module in the winter was possible and the engine functioned normally, while start-up in the summer time led to engine explosions.

This is explained, firstly, by the fact that the maximum pressure in the combustion chamber at the charge temperature T_3 = +20^{0}C exceeds the maximum permissible pressure of the engine body equal to P_{add}= 160 MPa , secondly, in fact that the value of the maximum pressure drop can exceed the ultimate strength of solid fuel, which decreases with increasing temperature.

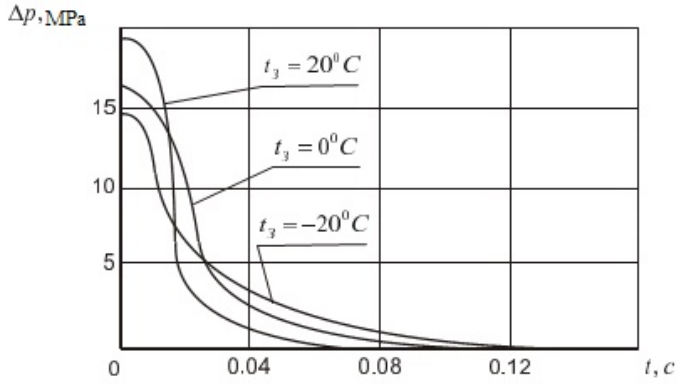

Fig. 4 – The dependence of the pressure drop at the ends of the charge from time to different values at the initial temperature of the charge

The diameter of the nozzle's critical section and the Poisson's ratio of the fuel material for given dimensions of the charge and the combustion chamber determine the ratio of the critical section area to the free-flow area of gases.

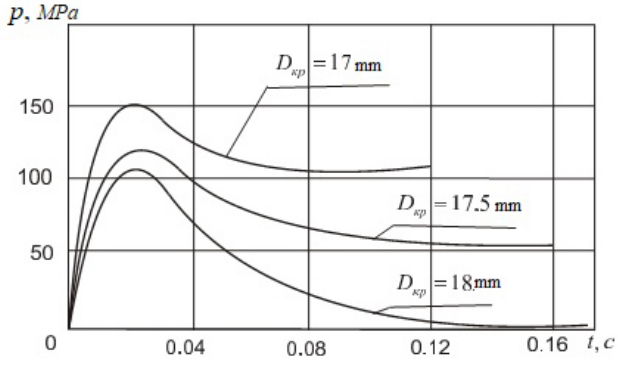

Fig. 5 – The change in pressure in the CC in time for different values of the diameters of the nozzle

From the graphs it can be seen that for given sizes of the fuel charge and the combustion chamber, an increase in the critical section area leads, along with a decrease in the average pressure in the chamber, to an increase in the pressure drop at the bottom and at the nozzle, which under certain conditions leads to destruction of the charge and the engine.

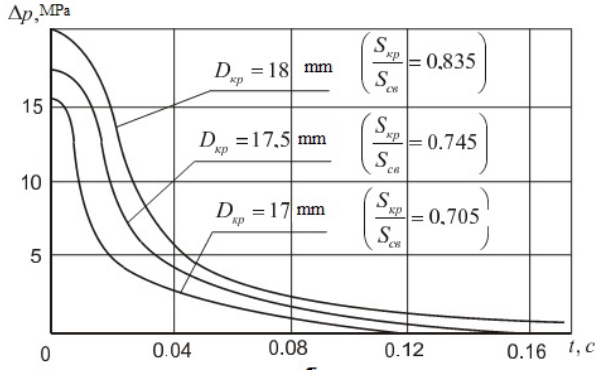

Fig. 6 –The dependence of the pressure drop at the ends of the charge over time for various values of diameters in critical sections

When approaching the ratio of the nozzle area to the area of free passage of gases to one, the operation condition of the fuel charge deteriorates dramatically, therefore, when designing solid propellant rocket engines with high charging density, special attention should be paid to the correct choice of this ratio.

In particular, when conducting experimental launches of modules "Grom-24" [31] with a nozzle of critical hole diameter d_{KP} = 17 mm , the engine worked fine, while replacing it with a nozzle of critical section diameter d_{KP} = 18 mm, led to the explosion of the engine.

4. CONCLUSIONS

– A construction scheme of a multi-modular reactive penetrator was proposed; it allows reaching greater depths compared to the classical scheme. The essential feature of the solid propellant solid propellant rocket engine is the fact that in the active part of the trajectory the solid propellant combustion products flow into the well formed during movement in the ground. During this, a number of processes arise due to the interaction of a supersonic high-temperature gas stream flowing out of a solid propellant nozzle with the borehole walls as a channel of variable length, which under certain conditions can lead to a change in flow parameters at the nozzle section, and, consequently, such important characteristics as *R* and a single impulse I_{ed}. The use of a multi-modular construction allows us to bypass this limitation, and in addition to ensure the operation of the engine in a less loaded mode. Moreover, the installation of the propulsion system in the process of penetration of the module into the ground has a significant impact on the stability of its movement, and with an increase in thrust, the trajectory of movement approaches a straight line.

– A method for calculating the gas-dynamic parameters of the working process in the solid-propellant engine of the lunar jet penetrator has been developed, which makes it possible at the initial design stage to determine the necessary requirements for the propulsion system and the conditions for the best way to deliver the instrument compartment to a given depth.

– A significant influence of charge of solid-fuel temperature on the nature and magnitude of the working pressure in the combustion chamber and the pressure drop at the bottom and the nozzle is shown. The launch of the penetrator at negative ambient temperatures was possible, and the engine functioned normally, while launches at positive temperatures led to engine explosions, since the maximum pressure in the combustion chamber exceeded the maximum permissible pressure of the engine construction.

When designing a penetrator engine with a high load density, special attention should be paid to the right choice of the ratio of the nozzle section area to the free-flow area of gases. Since the approximation of this ratio to one leads to a decrease in the average pressure in the combustion chamber and an increase in the pressure drop at the bottom and the nozzle, which negatively affects the working conditions of the engine.

ACKNOWLEDGEMENT

The study was done with a support of the state assignment of the Ministry of Science and Higher Education of the Russian Federation (code: 9.7969.2017/8.9).

REFERENCES

[1] V. V. Rodchenko, *Fundamentals of designing jet apparatus for movement in the ground*, MAI-PRINT, 2007.
[2] G. Weihrauch and E. Wollmann, Segmented penetrators, *Propellants, Explosives, Pyrotechnics*, vol. **18**, no. 5, pp. 270–274, 1993.

[3] S. V. Fedorov, V. A. Veldanov and N. A. Fedorov, About the possibility of increasing the depth of penetration into the soil-rock barriers of composite drummers with the tail section being shot during the interaction, *Bulletin MGTU them. N.E. Bauman. Series "Engineering"*, 2019, vol. 1, no. 124.

[4] A. S. Kurbatov, A. A. Orekhov and L. N. Rabinskiy, Solution of the problem of thermal stability of a thin-walled structure under non-stationary thermal action arising in the process of creating articles by the method of selective laser sintering, *Periodico Tche Quimica*, vol. **15**, Issue 1, pp. 441-447, 2018.

[5] V. F. Formalev and S. A. Kolesnik, Heat Transfer in a Half-Space with Transversal Anisotropy Under the Action of a Lumped Heat Source, *Journal of Engineering Physics and Thermophysics*, vol. **92**, no. 1, pp. 52-59, 2019.

[6] V. I. Krasovskii, I. N. Feofanov, S. I. Rasmagin, D. A. Zadorin, R. A. Zakharyan, M. A. Kazaryan, L. L. Chaikov, N. A. Bulychev, A. S. Averyushkin and B. A. Garibyan, Non-linear optical properties of nanosized metal oxide particles obtained in plasma discharge in liquid phase under ultrasonic cavitation, *Proceedings of SPIE*, vol. **10614**, article number 10614OZ, 2018.

[7] L.N. Rabinskiy and O.V. Tushavina, Experimental investigation and mathematical modelling of heat protection subjected to high-temperature loading, *Periodico Tche Quimica*, vol. **15**, Issue 1, pp. 321-329, 2018.

[8] A. S. Okonechnikov, L. N. Rabinskiy, D. V. Tarlakovskii and G. V. Fedotenkov, A nonstationary dynamic problem on the effects of surface loads on a half-space with a nanosized structure within the framework of the cosserat medium model, *International Journal of Nanomechanics Science and Technology*, vol. **7**, no. 1, pp. 61-75, 2016.

[9] S. A. Lurie, L. N. Rabinskiy, P. O. Polyakov, S. A. Sitnikov and Y. O. Solyaev, Mechanical properties of Si3 N4 -based composite ceramics with nanosized porosity, *International Journal of Nanomechanics Science and Technology*, vol. **8**, no. 4, pp. 347-358, 2017.

[10] A. V. Babaytsev, M. V. Prokofiev and L. N. Rabinskiy, Mechanical properties and microstructure of stainless steel manufactured by selective laser sintering, *International Journal of Nanomechanics Science and Technology*, vol. **8**, no. 4, pp. 359-366, 2017.

[11] M. V. Prokofiev, G. E. Vishnevskii, S. Y. Zhuravlev and L. N. Rabinskiy, Obtaining nanodispersed graphite preparation for coating ultrathin mineral fibers, *International Journal of Nanomechanics Science and Technology*, vol. **7**, no. 2, pp. 97-105, 2016.

[12] A. V. Babaytsev, M. V. Prokofiev and L. N. Rabinskiy, Mechanical properties and microstructure of stainless steel manufactured by selective laser sintering, *International Journal of Nanomechanics Science and Technology*, vol. **8**, no. 4, pp. 359-366, 2017.

[13] S. A. Lurie, L. N. Rabinskiy, P. O. Polyakov, S. A. Sitnikov and Y. O. Solyaev, Mechanical properties of Si3 N4 -based composite ceramics with nanosized porosity, *International Journal of Nanomechanics Science and Technology*, vol. **8**, no. 4, pp. 347-358, 2017.

[14] Ek. L. Kuznetsova, E. L. Kuznetsova, L. N. Rabinskiy and S. I. Zhavoronok, On the equations of the analytical dynamics of the quasi-3D plate theory of I. N. Vekua type and some their solutions, *Journal of Vibroengineering*, vol. **20**, no. 2, pp. 1108-1117, 2018.

[15] A. N. Danilin, E. L. Kuznetsova, N. N. Kurdyumov, L. N. Rabinskiy and S. S. Tarasov, A modifiedbouc-wen model to describe the hysteresis of non-stationary processes, *PNRPU Mechanics Bulletin*, no. 4, pp. 187-199, 2016.

[16] A. N. Danilin, N. N. Kurdumov, E. L. Kuznetsova and L. N. Rabinsky, Modelling of deformation of wire spiral structures, *PNRPU Mechanics Bulletin*, no. 4, pp. 72-93, 2015.

[17] A. N. Danilin, E. L. Kuznetsova, N. N. Kurdyumov, L. N. Rabinskiy and S. S. Tarasov, A modifiedbouc-wen model to describe the hysteresis of non-stationary processes, *PNRPU Mechanics Bulletin* no. 4, pp. 187-199, 2016.

[18] N. A. Bulychev, E. L. Kuznetsova, V. V. Bodryshev and L. N. Rabinskiy, Nanotechnological aspects of temperature-dependent decomposition of polymer solutions, *Nanoscience and Technology: An International Journal*, vol. **9**, no. 2, pp. 91-97, 2018.

[19] V. F. Formalev and S. A. Kolesnik, Analytical investigation of heat transfer in an anisotropic band with heat fluxes assigned at the boundaries, *Journal of Engineering Physics and Thermophysics*, vol. **89**, no. 4, pp. 975-984, 2016.

[20] V. F. Formalev and S. A. Kolesnik, On Inverse Coefficient Heat-Conduction Problems on Reconstruction of Nonlinear Components of the Thermal-Conductivity Tensor of Anisotropic Bodies, *Journal of Engineering Physics and Thermophysics*, vol. **90**, no. 6, pp. 1302-1309, 2017.

[21] V. F. Formalev, S. A. Kolesnik and E .L. Kuznetsova, Analytical study on heat transfer in anisotropic space with thermal conductivity tensor components depending on temperature, *Periodico Tche Quimica*, vol. **15**, issue 1, pp. 426-432, 2018.

[22] L. N. Rabinsky and O. V. Tushavina, Mathematical modeling and experimental studies of thermal protection of composite materials under high-intensity effects, taking into account thermal diffusion, *STIN*, vol. **4**, pp. 22-26.
[23] V. V. Rodchenko, E. R. Sadretdinova, V. A. Zagovorchev and A. V. Galeev, The Selection of Terrestial Soil-Analogs as a Medium for Movement of Lunar Reactive Penetrator, *International Journal of Alternative Energy and Ecology*, vol. **28**-**30**, no. 240-242, pp. 69-81, 2017.
[24] A. Tate, A theory for the deceleration of long rods after impact, *Journal of the Mechanics and Physics of Solids*, vol. **15**, issue 6, pp. 387-399.
[25] V. V. Rodchenko, E. R. Sadretdinova and E. V. Gusev, The choice of parameters of the penetrator for the study of the lunar soil, *Bulletin of the Moscow Aviation Institute*, vol. **17**, no. 3, 2010.
[26] V. V. Rodchenko, E. V. Gusev, A. G. Galeev and E. R. Sadretdinova, *The choice of parameters of the penetrator entering the lunar soil at zero speed*, Trudy MAI.
[27] V. A. Veldanov, V. E. Smirnov and O. B. Khavroshkin, Lunar penetrator: Reducing overload and penetration control, *Solar System Research*, vol. **33**, no. 5, pp. 432-436, 1999.
[28] A. M. Lipanov and Yu. M. Milekhin, (eds.) *Internal ballistics of solid-propellant pocket engines*, Mashinostroenie, 2007.
[29] V. G. Kazantsev and M. P. Karputin, Application of fracture mechanics to choose the rational varients of design elements in solid propellant rocket motor grains, *Vestnik Permskogo natsional'nogo issledovatel'skogo politekhnicheskogo universiteta. Aerokosmicheskaya tekhnika*, no. 41, pp. 139-157, 2015.
[30] R. E. Sorokin, *Gas thermodynamics of solid-fuel rocket engines*, Nauka, 1967.
[31] A. N. Astapov, D. V. Nushtaev and L. N. Rabinskiy, Forecasting of thermal stress and adhesion in non-canonical substrate – Coating system, *Periodico Tche Quimica*, vol. **15**, Issue 1, pp. 448-463, 2018.